Intuitive Formulation of Discontinuous Galerkin Surface Integral Equations for Electromagnetic Scattering Problems

Gaobiao Xiao, *Member, IEEE*, and Yibei Hou, *Student Member, IEEE*

***Abstract*— An intuitive formulation of discontinuous Galerkin surface integral equation (DG-SIE) method is proposed in this paper, which is established by performing singularity extraction and singling out the infinitely large term in the entries of the impedance matrices associated with the SIEs, which are popular in solving electromagnetic scattering problems. Nonoverlapping trial and test functions defined on triangles are employed without requirements of the surface current (normal) continuity across their internal boundary contours. The proposed SIE-DG formulation is very flexible and is validated by examples of perfect electrically conducting targets in both conformal and nonconformal meshes.**

***Index Terms*— Discontinuous Galerkin (DG) method, discontinuous vector basis function (DVBF), surface integral equation (SIE).**

I. Introduction

Surface integral equation formulations are popular in solving electromagnetic scattering problems of perfect electrically conducting (PEC) objects or homogeneous media. To solve the surface integral equations (SIEs) with the conventional Galerkin scheme, div-conforming basis functions, such as Rao–Wilton–Glisson (RWG) basis functions [1], are usually employed for the trial and test functions, and the continuity of the normal components of the surface currents across internal edges is enforced automatically. In analyzing large-scale systems, domain decomposition is perhaps the most effective technique [2]–[5]. In practical engineering, a large system is usually divided into many subblocks, and each subblock is modeled using a general computer-aided-design (CAD) tool with its geometrical data stored in standard file formats, such as SAT, SLD, and SM2. For example, an aircraft is usually modeled using PEC surfaces, and the data of its body, wings, and engines can be stored in different SAT files. When performing electromagnetic analysis, we have to import these data files and combine them to form a connected PEC object. However, because of the limited modeling accuracy of CAD tools, two pieces of surface may not be perfectly connected: their interfacing boundaries do not coincide at the connection edges or tearing lines. There are possibly some misplacement at the interfacing edges, which will cause spurious slits or overlaps. Adjustment of the abnormal meshes at the connections is usually required before analyzing the object. Obviously, it is more efficient if we can directly combine every subdomain together and mesh each subblock separately without the necessity to correct the displacement. However, a troublesome issue is that in these situations, the mesh structure would be nonconformal at the connecting boundaries. Nonconformal mesh structures are also well encountered when we make local mesh refinement or analyze multiscale problems. Unfortunately, the numerical accuracy could be degraded if nonconformal meshes are adopted, because it is difficult to define div-conforming vector basis functions on the mesh and the couplings between nonconformal mesh elements are more difficult to be evaluated accurately.

Thanks to the discontinuity of the approximation, discontinuous Galerkin (DG) method shows great adaptability to complex geometries through the use of unstructured possibly nonconformal meshes. Galerkin methods for elliptic and parabolic equations using discontinuous finite elements were independently proposed in [6]–[8], which were then called interior penalty (IP) methods. Meanwhile, the DG methods for hyperbolic equations have also been developed [10]. A comprehensive review of these methods can be found in [11]–[13]. Recently, DG methods have been applied to solving Maxwell's equations in the framework of finite element method (FEM) [14]–[17]. In spite of this, DG methods have also been extended to SIEs for electromagnetic scattering problems [18]–[23]. DG methods can be applied to various types of elements, nonconformal meshes, and nonuniform orders of approximations [24]. The continuities of the currents and boundary conditions are enforced weakly through the Galerkin testing schemes, and the choice of basis functions becomes very flexible.

The discontinuous Galerkin surface integral equation (DG-SIE) method, referred to as IEDG in [22], is formulated by introducing an IP term, which was inspired by the DG in FEM. In the method, discontinuous vector basis functions (DVBFs) have been adopted, and have shown great flexibility in handling large-scale electromagnetic systems. However, the IP term is not considered in [23]. The error due to this simplification is not severe, because a good strategy has been utilized in [23]: nonconformal bases and DG method are used only at the connecting boundaries, while RWG bases and the conventional Galerkin method are used for all other normal surfaces.

Manuscript received August 18, 2015; revised July 17, 2016; accepted November 10, 2016. Date of publication November 17, 2016; date of current version January 2, 2017. This work was supported by the National Science Foundation of China under Grant 61234001 and Grant SAST804-201505.

The authors are with the Electronic Engineering Department, Shanghai Jiao Tong University, Shanghai 200240, China (e-mail: gaobiaoxiao@sjtu.edu.cn).

Color versions of one or more of the figures in this paper are available online at http://ieeexplore.ieee.org.

Digital Object Identifier 10.1109/TAP.2016.2630501

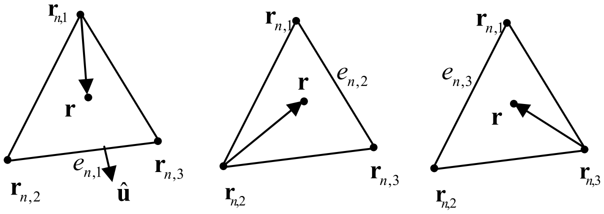

Fig. 1. Three DVBFs on a triangle.

In this paper, we will present an intuitive formulation of DG for SIEs, which is different from that described in [22] and [23]. As is well known, if DVBFs are utilized, the discontinuity of the surface currents will cause accumulation of charges on the edges of the mesh elements. As a result, the mutual coupling of adjacent elements tends to be infinitely large if the two accumulated line charges coincide. In the DG-SIEs described in [22], the unbounded line–line integral is dropped and an IP term is introduced to penalize the potential produced by the charges accumulated along the edges. However, in the proposed method, the core term that makes the mutual coupling infinitely large is singled out. After that, the coupling is, in some extent, loosened by deleting a small integration range in the neighborhood of the singular point. The new DG formulation can be applied to solving the surface electric field integral equation (EFIE), the surface magnetic field integral equation (MFIE), and the surface combined field integral equation (CFIE). Analysis shows that the accuracy and the conditioning of the new DG-SIEs can be controlled by adjusting the coupling intensity, and no IP term is necessary to be introduced. For the sake of simplicity, hereafter, we use EFIE-DG, MFIE-DG, and CFIE-DG to, respectively, denote the method of solving the three SIEs using DVBFs and DG testing scheme, while EFIE-RWG, MFIE-RWG, and CFIE-RWG for the methods of solving the three SIEs with RWG bases and conventional Galerkin testing scheme.

The formulation for EFIE-DG is detailed in Section II, which is extended to MFIE-DG and CFIE-DG in Section III. Numerical examples are presented in Section IV, with the conclusions drawn in Section V.

II. Intuitive Formulation of Discontinuous Galerkin Surface Electric Field Integral Equation

The nonoverlapped DVBFs employed in this paper are defined on a triangle, as shown in Fig. 1.

There are three basis functions $\mathbf{f}_{n,q}, q = 1, 2, 3$ being defined on the triangle S_n. Their expressions are similar to that of a half-RWG (HRWG) basis function, which can be written explicitly as follows:

$$\mathbf{f}_{n,q} = \begin{cases} \dfrac{l_{n,q}}{2A_n}(\mathbf{r} - \mathbf{r}_{n,q}), & \mathbf{r} \in S_n \\ 0, & \text{elsewhere} \end{cases}, \quad q = 1, 2, 3 \tag{1}$$

where $\mathbf{r}_{n,q}$ is the qth node on the triangle S_n and $l_{n,q}$ is the length of its opposite edge $e_{n,q}$. A_n is the area of the triangle. $\hat{\mathbf{u}}$ is the binormal unit vector (or called the in-plane normal unit) of edge $e_{n,q}$. For the sake of convenience, hereafter, the node $\mathbf{r}_{n,q}$ and the edge $e_{n,q}$ are referred to as the reference node and reference edge of the basis function $\mathbf{f}_{n,q}$, respectively.

The divergence of the discontinuous basis function is associated with the charge density, which can be derived as

$$\nabla_s \cdot \mathbf{f}_{n,q} = \begin{cases} \dfrac{l_{n,q}}{A_n} - \delta(\mathbf{r} - \mathbf{r}_{e_{n,q}}), & \mathbf{r} \in S_n \\ 0, & \text{elsewhere} \end{cases} \tag{2}$$

where $\delta(\mathbf{r} - \mathbf{r}_{e_{n,q}})$ is the Dirac delta function. For any given smooth function $v(\mathbf{r})$ on surface S containing edge $e_{n,q}$, there exists the following integral equality:

$$\int_S v(\mathbf{r})\delta(\mathbf{r} - \mathbf{r}_{e_{n,q}})dS = \int_{e_{n,q}} v(\mathbf{r})dl. \tag{3}$$

Obviously, the electric charge corresponding to the basis function $\mathbf{f}_{n,q}$ consists of two parts: a constant surface charge on the triangle with density of $[-(j\omega\varepsilon)^{-1}(l_{n,q}/A_n)]$ and a line charge with density of $[(j\omega\varepsilon)^{-1}]$ on the edge where the current is terminated.

Consider a PEC object with its surface $\partial\Omega$ being discretized into N triangles and $\partial\Omega = S_1 \cup S_2 \cdots \cup S_N$. Therefore, there are totally $3N$ DVBFs as defined in (1). The surface electric current can be approximated as

$$\mathbf{J}_s(\mathbf{r}) = \sum_{n=1}^{N}\sum_{q=1}^{3} j_{n,q}\mathbf{f}_{n,q}(\mathbf{r}). \tag{4}$$

Two surface trace operators on $\partial\Omega$ are introduced [14]: the tangential components trace operator $\pi_\tau(\cdot)$ and the twisted tangential trace operator $\gamma_\tau(\cdot)$, which are denoted as

$$\pi_\tau(\mathbf{u}) = \hat{n} \times (\mathbf{u} \times \hat{n})|_{\partial\Omega}, \quad \gamma_\tau(\mathbf{u}) = \hat{n} \times \mathbf{u}|_{\partial\Omega}. \tag{5}$$

The electric field integral equation (EFIE) can be established on a PEC surface

$$\pi_\tau[\mathbf{E}^{\text{inc}}(\mathbf{r})] + \pi_\tau[\mathcal{L}\{\mathbf{J}_s\}] = 0, \quad \mathbf{r} \in \partial\Omega \tag{6}$$

where $\mathcal{L}$ is the electric field integral operator and can be represented as

$$\mathcal{L}\{\mathbf{J}_s\} = -j\omega\mathbf{A}\{\mathbf{J}_s\} - \nabla\phi\{\mathbf{J}_s\} \tag{7}$$

with

$$\mathbf{A}\{\mathbf{J}_s\} = \mu\int_{\partial\Omega} g(\mathbf{r};\mathbf{r}')\mathbf{J}_s(\mathbf{r}')dS' \tag{8}$$

$$\phi\{\mathbf{J}_s\} = -\frac{1}{j\omega\varepsilon}\int_{\partial\Omega} g(\mathbf{r};\mathbf{r}')\nabla_s' \cdot \mathbf{J}_s(\mathbf{r}')dS'. \tag{9}$$

Here, $R = |\mathbf{r} - \mathbf{r}'|$, and $g(\mathbf{r};\mathbf{r}') = e^{-jkR}/4\pi R$ is the scalar Green's function in free space. μ and ε are the permeability and the permittivity in the free space, respectively.

In DG method, the trial function space $\oplus_{m=1}^{N}\oplus_{p=1}^{3}\mathbf{f}_{m,p}$ is allowed to be discontinuous across the internal triangle edges. Testing (6) with the discontinuous basis functions yields

$$\left\langle \mathbf{f}_{m,p}, \sum_{n=1}^{N}\sum_{q=1}^{3} j_n\pi_\tau[\mathcal{L}\{\mathbf{f}_{n,q}\}]\right\rangle_{S_m} = -\left\langle \mathbf{f}_{m,p}, \pi_\tau\left[\mathbf{E}_m^{\text{inc}}(\mathbf{r})\right]\right\rangle_{S_m} \tag{10}$$

in which the surface inner product is defined by

$$\langle \mathbf{v}, \mathbf{u} \rangle_{S_m} = \int_{S_m} (\mathbf{v} \cdot \mathbf{u}) dS. \tag{11}$$

The scalar potential contributed from the surface charge density and the line charge density can be separated as follows:

$$\phi\{\mathbf{f}_{n,q}\} = \phi_{S_n}\{\mathbf{f}_{n,q}\} + \phi_{C_n}\{\mathbf{f}_{n,q}\} \tag{12}$$

where

$$\begin{aligned}\phi_{S_n}\left\{\nabla_s' \cdot \mathbf{f}_{n,q}\right\} &= -\frac{1}{j\omega\varepsilon} \int_{S_n} g(\mathbf{r}; \mathbf{r}') \nabla_s' \cdot \mathbf{f}_{n,q} dS' \\ \phi_{C_n}\{\hat{\mathbf{u}}_{n,q} \cdot \mathbf{f}_{n,q}\} &= \frac{1}{j\omega\varepsilon} \int_{e_{n,q}} g(\mathbf{r}; \mathbf{r}') (\hat{\mathbf{u}}_{n,q} \cdot \mathbf{f}_{n,q}) dl'.\end{aligned} \tag{13}$$

The property of $(\hat{\mathbf{u}}_{n,q} \cdot \mathbf{f}_{n,q}) = 0$ when $\mathbf{r}' \in C_n \backslash e_{n,q}$ has been used to derive (13).

The Green's identity is often applied to reducing the order of singularity in testing the scalar potential. Although it is quite fundamental, we write one entry of (10) explicitly as follows:

$$\begin{aligned}\langle \mathbf{f}_{m,p}, \pi_\tau[\mathcal{L}\{\mathbf{f}_{n,q}\}] \rangle_{S_m} = {} & \langle \mathbf{f}_{m,p}, -j\omega \mathbf{A}\{\mathbf{f}_{n,q}\} \rangle \\ & + \langle \nabla_s \cdot \mathbf{f}_{m,p}, \phi_{S_n}\left\{\nabla_s' \cdot \mathbf{f}_{n,q}\right\} \rangle_{S_m} \\ & + \langle \nabla_s \cdot \mathbf{f}_{m,p}, \phi_{C_n}\{\hat{\mathbf{u}}_{n,q} \cdot \mathbf{f}_{n,q}\} \rangle_{S_m} \\ & - \langle \hat{\mathbf{u}}_{m,p} \cdot \mathbf{f}_{m,p}, \phi_{S_n}\left\{\nabla_s' \cdot \mathbf{f}_{n,q}\right\} \rangle_{C_m} \\ & - \langle \hat{\mathbf{u}}_{m,p} \cdot \mathbf{f}_{m,p}, \phi_{C_n}\{\hat{\mathbf{u}}_{n,q} \cdot \mathbf{f}_{n,q}\} \rangle_{C_m}.\end{aligned} \tag{14}$$

Obviously, it can be seen that the first two terms in the right-hand side have exactly the same integration forms as those in the conventional Galerkin method, while the last three terms are caused by the discontinuity of the basis functions. If we interpret the test function $\mathbf{f}_{m,p}$ as a surface current, then the first term in the right-hand side can be viewed as the total magnetic energy when the current is put into the vector potential created by the electric current $\mathbf{f}_{n,q}$; similarly, the second and the third term can be regarded, respectively, as the electric energy when the surface electric charge associated with $\mathbf{f}_{m,p}$ is put in the scalar potential generated by the surface charge associated with $\mathbf{f}_{n,q}$ and the line charge on edge $e_{m,p}$; the fourth and the last term can be regarded, respectively, as the electric energy when the line electric charge on the edge $e_{m,p}$ is put in the potential due to the surface charge associated with $\mathbf{f}_{n,q}$ and the line charge on the edge $e_{n,q}$. The sum of these electromagnetic energies should be equal to the total energy supplied by the incident field, which is $\langle \mathbf{f}_{m,p}, \pi_\tau[\mathbf{E}_m^{\text{inc}}(\mathbf{r})] \rangle_{S_m}$. It can be checked that in all situations, the first four terms of energies are bounded. However, the last term may become infinitely large when the two line charges coincide, which will make the conventional Galerkin testing scheme not applicable without modification.

In the conventional continuous Galerkin (CG) method, the surface current continuity is forced by using RWG bases, while in DG, discontinuous basis functions are used, so the surface currents are not necessary to be strictly continuous across triangle edges. However, the surface currents are made to be approximately continuous by introducing an IP term in [22] and a Δ-term in the method proposed in this paper, which is associated with the singularity of the last term in (14). It is noticed that the dual contour line integral on both sides of the contour can be canceled in the traditional CG method employing RWGs in conformal meshes, so that no charges accumulate along the contour.

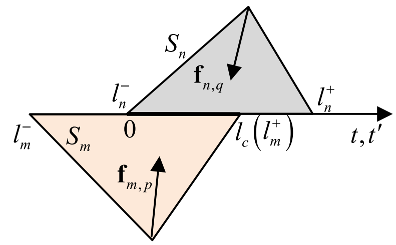

Fig. 2. Local coordinate system for two discontinuous basis functions sharing a common edge.

Equation (14) is almost the same as [22, eqs. (22) and (23)]. Both Peng *et al.*'s work [22] and the method proposed here are focused on seeking an efficient method to treat the unbounded line–line integral in (14) via the concept of DG. The infinite double contour integral terms are cancelled in [22], and for compensation, an IP term is added to penalize the accumulation of charges across the contour boundary. An IP stabilization function is introduced to decide the strength of the penalization. Different from Peng *et al.*'s work [22], we are intended to evaluate the infinitely large term in (14) by an approximate scheme rather than replacing this term by an IP term according to the idea of DG.

In order to establish a feasible testing scheme using DVBFs, the last term will be checked in more details. Consider two basis functions $\mathbf{f}_{m,p}$ and $\mathbf{f}_{n,q}$, whose reference edges are put in the local coordinate system shown in Fig. 2. The t-axis is for the field edge, and the t'-axis for the source edge. The two axes coincide and share a common origin. The reference edge $e_{m,p}$ spans over $[l_m^-, l_m^+]$, and $e_{n,q}$ over $[l_n^-, l_n^+]$. We have assumed $l_n^- = 0$ and $l_m^+ = l_c$, so the common interface shared by the two reference edges is located in the interval $[0, l_c]$. The last term of (14) is a double-folded line integration on the two reference edges. Since it is not difficult to find that only the integration over the interval $[0, l_c]$ tends to be infinitely large, the integration can be written with the technique of singularity extraction as follows:

$$\begin{aligned}&\frac{1}{j\omega\varepsilon} \int_0^{l_c} \int_0^{l_c} \frac{e^{-jk|t-t'|}}{4\pi|t-t'|} dt' dt \\ &\quad = \frac{1}{j\omega\varepsilon} \int_0^{l_c} \int_0^{l_c} \frac{e^{-jk|t-t'|} - 1}{4\pi|t-t'|} dt' dt \\ &\qquad + \frac{1}{j\omega\varepsilon} \int_0^{l_c} \int_0^{l_c} \frac{1}{4\pi|t-t'|} dt' dt.\end{aligned} \tag{15}$$

The first term at the right-hand side of (15) is bounded and can be calculated by using the Gaussian quadrature integration formulas, while the second term is unbounded and can be made bounded by deleting a small interval $[t-\Delta, t+\Delta]$ in the neighborhood of the singular point $(1/|t-t'|)$. It is reasonable to assume that the value of Δ should be much smaller than l_c; hence, the second term of the right-hand side of (15) can be approximately integrated directly as follows:

$$\begin{aligned}\int_0^{l_c}\int_0^{l_c}\frac{1}{4\pi|t-t'|}dt'dt &\approx \int_\Delta^{l_c-\Delta}\left[\int_0^{t-\Delta}\frac{1}{t'-t}dt'+\int_{t+\Delta}^{l_c}\frac{1}{t-t'}dt'\right]dt \\ &= 2l_c(\ln l_c-1)-2l_c\ln\Delta.\end{aligned}\tag{16}$$

Obviously, we have $\lim_{\Delta\to 0}(l_c\ln\Delta)=\infty$. It has to be noted that the small interval is removed only in performing the integration of (16), while it is not removed for other line integrations in (14). It can be demonstrated that except this Δ-term, the other parts of the integration in (14) do not contain Δ and are all bounded in all situations. Since $l_c\ln\Delta=0$ for $l_c=0$, the Δ-term $(2l_c\ln\Delta)$ is not zero only when the reference edges of the two DVBFs share a common interfacing line segment with length of l_c. Therefore, the matrix form of (10) can be written in the following form:

$$(\mathbf{Z}_{\text{EFIE}}+\alpha\mathbf{Z}_\Delta)\cdot\mathbf{I}=\mathbf{e}_{in}\tag{17}$$

where $\alpha=(\ln\Delta)/(\omega\varepsilon)$ and $\mathbf{I}=[j_1,j_2,\ldots]^t$. The entries of the matrix $\mathbf{Z}_{\text{EFIE}}$ contain all the integration value of (14) except the term that contains $(l_c\ln\Delta)$. The entries of $\mathbf{Z}_\Delta$ can be derived as

$$Z_\Delta(\tilde{m},\tilde{n})=\begin{cases}\dfrac{jl_c}{2\pi}, & e_{m,p}, e_{n,q}\text{share common edge } l_c\\ 0, & \text{otherwise}\end{cases}\tag{18}$$

where $\tilde{m}$ and $\tilde{n}$ are the sequential numbers of the discontinuous basis functions $\mathbf{f}_{m,p}$ and $\mathbf{f}_{n,q}$, respectively.

Judging from (18), we can see that $\mathbf{Z}_\Delta$ is a symmetrical matrix, and each row of $\mathbf{Z}_\Delta$ contains only several nonzero elements, corresponding to the DVBFs whose reference edges share a common interface. In order to get a more clear understanding, let us consider applying DG to a conformal triangular mesh structure, where two internal DVBFs that share a common reference edge can form an RWG. In this case, each row of $\mathbf{Z}_\Delta$ contains only two nonzero elements of identical value, corresponding to the positive and negative part of an RWG basis. Assume that only the p_0th and the q_0th element are nonzero in the $\tilde{m}$th row of $\mathbf{Z}_\Delta$, which are, respectively, associated with the current expansion coefficient j_{p_0} and j_{q_0}. The two nonzero elements can be readily derived from (18) as

$$\alpha Z_\Delta(\tilde{m},p_0)=\alpha Z_\Delta(\tilde{m},q_0)=(\ln\Delta)(jl_{c_0}/2\pi\omega\varepsilon)$$

where l_{c_0} is the common interface of the two discontinuous vector bases. (It is also the common edge of the RWG basis formed by the two DVBFs.) We can spell out the $\tilde{m}$th equation in the matrix system as follows:

$$\begin{aligned}\sum_{\tilde{m}\neq p_0,\tilde{n}\neq q_0} Z(\tilde{m},\tilde{n})j_n+(\ln\Delta)\left(\frac{jl_{c_0}}{2\pi\omega\varepsilon}\right)(j_{p_0}+j_{q_0})\\ =e_{in}(\tilde{m}).\end{aligned}\tag{19}$$

When $\Delta\to 0$, we have $\ln\Delta\to\infty$. Since $e_{in}(\tilde{m})$ is bounded, (19) requires that $j_{p_0}+j_{q_0}\to 0$, which means that the expansion coefficients of any pair of two DVBFs whose reference edges coincide must have equal amplitude but opposite sign. Thus, the two DVBFs almost exactly behave like a standard RWG basis function. The surface current is forced to be normally continuous across all internal edges; therefore, all the line integrations in (14) will vanish and the solution will be the same as that obtained using RWG bases. In other words, if we make $\Delta\to 0$, (17) will guarantee the continuity of the normal components of the surface current across internal edges, so the solution to (17) should approach to that of the standard EFIE using RWG bases. However, the condition number of the coefficient matrix in (17) is much larger due to the property of the DVBFs, which can be verified from the Gram matrix of the basis functions. Although the above-mentioned conclusion is drawn from conformal meshes, it is valid for nonconformal meshes, i.e., by setting $\Delta\to 0$, we can make the normal component of the surface current continuous across internal edges.

For $0<\Delta\ll l_c$, α is bounded. It can be considered as that the mutual coupling between two coincided line charges is loosened from infinitely large to a finite level, so the surface current can be discontinuous across edges. If larger Δ is used, the mutual coupling is made looser, and the surface currents tend to become more discontinuous across internal edges.

As has been discussed previously, the solution to (17) approaches to that obtained using RWG bases in conjunction with the conventional Galerkin method. However, it is not necessary that the accuracy of DG is always worse than that of the conventional Galerkin method. In DG methods where DVBFs are used, it is possible that local discontinuity may bring higher global approximation accuracy.

Empirically, we suggest to choose $0<\Delta<l_{\min}/10$, where $l_{\min}$ is the minimum length of edge in the mesh. Larger Δ may cause larger numerical errors.

III. DG Formulation for MFIE and CFIE

The surface magnetic field integral equation for PEC object takes the usual form of

$$\gamma_\tau[\mathcal{K}\{\mathbf{J}_s\}]=-\gamma_\tau[\mathbf{H}^{\text{inc}}(\mathbf{r},t_j)],\quad \mathbf{r}\in\partial\Omega.\tag{20}$$

In this paper, the combined field integral equation is obtained by combining the EFIE and the MFIE in the following form:

$$\begin{aligned}\pi_\tau[\mathcal{L}\{\mathbf{J}_s\}]+\eta\gamma_\tau[\mathcal{K}\{\mathbf{J}_s\}]\\ =-\pi_\tau[\mathbf{E}^{\text{inc}}(\mathbf{r})]-\eta\gamma_\tau[\mathbf{H}^{\text{inc}}(\mathbf{r},t_j)],\ \mathbf{r}\in\partial\Omega\end{aligned}\tag{21}$$

where

$$\mathcal{K}\{\mathbf{J}_s\}=\frac{1}{\mu}\nabla\times\mathbf{A}\{\mathbf{J}_s\}=\int_{\partial\Omega}\nabla g(\mathbf{r};\mathbf{r}')\times\mathbf{J}_s(\mathbf{r}')dS'.\tag{22}$$

Using the DVBFs as expansion and testing functions, (20) and (21) can be discretized to their matrix forms just like handling the EFIE. The resultant matrix equations are

$$\mathbf{Z}_{\text{MFIE}}\cdot\mathbf{I}=\mathbf{h}_{\text{in}}\tag{23}$$

$$(\mathbf{Z}_{\text{CFIE}}+\alpha\mathbf{Z}_\Delta)\cdot\mathbf{I}=\mathbf{e}_{\text{in}}+\eta\mathbf{h}_{\text{in}}\tag{24}$$

where α and $\mathbf{Z}_\Delta$ are the same as defined previously. The formulation can be justified by checking that all the double-folded integrations associated with the operator $\mathcal{K}\{\mathbf{J}_s\}$ are bounded.

Close examination shows that the term associated with $\alpha\mathbf{Z}_\Delta$ is practically very similar to the contour internal penalty term introduced in [22] (refer to [22, eq. (36)]), which was inspired by the IP-DG methods. Obviously, the constant α corresponds to the internal penalty stabilization function β defined in [22]. Note that we have used $\hat{\mathbf{u}}_m$ instead of $\hat{\mathbf{t}}_{mn}$ in [22] to denote the in-plane normal unit. However, in this paper, the term $\alpha\mathbf{Z}_\Delta$ is derived directly by singling out the singular term in the integral accounting for the mutual coupling of the two overlapped line charges caused by the discontinuity of the surface currents. The constant α is clearly in proportional to $\ln\Delta$, and is perhaps more intuitive than the concept of internal penalty.

IV. Numerical Examples

In this section, PEC scatterers in the 3-D free space are used to verify the method of EFIE-DG and CFIE-DG. It is noted that HRWGs (DVBFs) are used in the three SIE-DG methods while RWGs are adopted in SIE-RWG methods in the following descriptions. Assume that an incident plane wave with an amplitude of 1 V/m illuminates on the scatterers along the z-axis. In order to compare the numerical accuracy, we define a relative root mean square (rms) error for X with respect to Y as follows:

$$\mathrm{Err} = 20\log(\|\mathrm{X\text{-}Y}\|/\|\mathrm{Y}\|) \tag{25}$$

where $\|\cdot\|$ means the rms. X and Y can be the surface currents or the radar cross sections (RCSs).

Example A (PEC Sphere With Conformal Mesh): The PEC sphere considered here has a radius of 1 m. Its surface is discretized into a conformal triangular mesh with 2304 triangles, and 3456 RWGs will be generated. The ratio of the maximum edge length versus the minimum edge length is 2.78. The frequency of the incident plane wave is 100 MHz.

Every RWG basis is separated into two parts to get two DVBFs. The sign of the negative HRWG is changed, so that the reference direction in every discontinuous vector basis points away from its reference node, as defined in Fig. 1. Consequently, totally 6912 DVBFs are obtained.

To reveal the effect of Δ, we decrease Δ from $l_{\min}$ to about $(10^{-8}l_{\min})$, or equivalently to increase $(-\ln\Delta)$ from 4 to 20. The relative errors of the surface current expansion coefficients obtained using EFIE-DG and EFIE-RWG are compared in Fig. 3, where the term J_{err} is used and defined according to (25). It can be seen that, with the decreasing of Δ, the results obtained by using EFIE-DG approach more and more close to those obtained using EFIE-RWG, which has verified the observation described previously. The relative error for the current coefficients obtained with CFIE-DG versus that obtained using EFIE-RWG is also shown in Fig. 3, which shows that the CFIE-DG formulation is feasible. Although not shown in Fig. 3, the relative error associated with MFIE-DG is calculated to be about -44 dB. It does not vary with $\ln\Delta$, as can be seen from (23). Meanwhile, we have checked that if we simply discard the singular double-folded line integration, as proposed in [23], the relative error is about -28 dB.

The condition numbers of the EFIE-SIEs are shown in Fig. 4. Except at small Δ, the condition number associated with the EFIE-DG is usually larger than that associated with the corresponding EFIE-RWG.

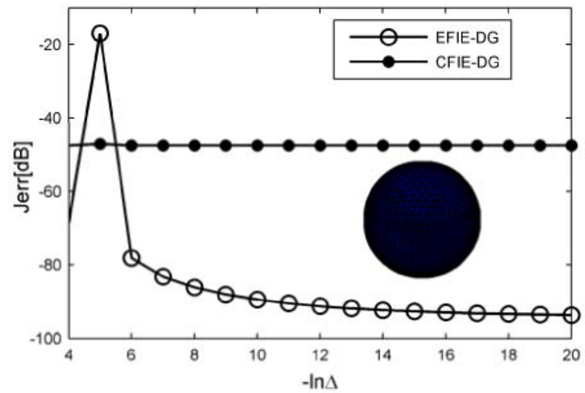

Fig. 3. Variation of the relative errors of the surface current versus Δ. RWG bases are used in EFIE-RWG, and DVBFs are used in EFIE-DG.

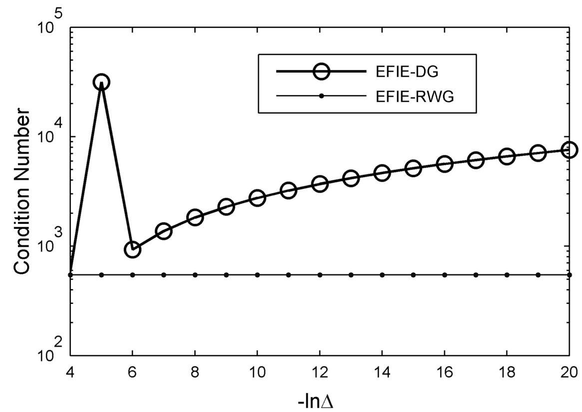

Fig. 4. Variation of the condition numbers versus Δ.

The double-folded integrations in (14) are performed using Gaussian quadrature formulas. When the field point is very close to the source point, singularity extraction techniques should be applied. For surface integrations, a well-adopted strategy is to evaluate the inner-fold integration using singularity extraction [25]–[27] and evaluate the outer-fold integration using Gaussian quadrature formulas directly. However, this strategy has to be modified for the line integrations, because the inner-fold line integration value is infinitely large when the field and source point coincide, for example, two edges share a common interface or connect at one end. The former case has been addressed in Section II, where the double-folded line integration tends to be infinitely large and should be evaluted with (15) and (16). As for the later case, although the double-folded line integration is bounded, the accuracy is not good if we use the Gaussian quadrature to evaluate the inner integration directly, because the inner-fold line integration is infinitely large at the connecting point. An effective method is to separate the singular part of the inner integrant at the connecting piont and analytically evaluate its double-folded line integration instead of analytically performing the inner-fold integration alone. Based on the same reason, it is more efficient to change the integration order of the third term

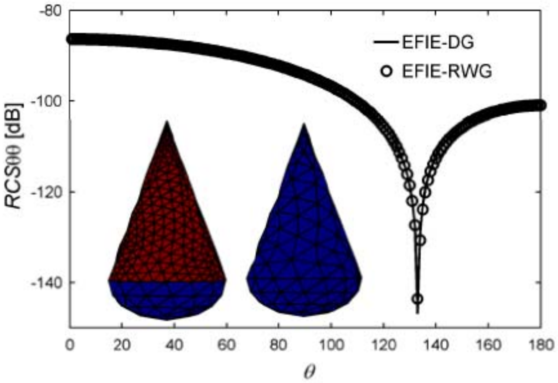

Fig. 5. RCS$\theta\theta$ of the PEC cone sphere. EFIE-DG: DVBF and DG method. EFIE-RWG: RWG bases and conventional Galerkin method.

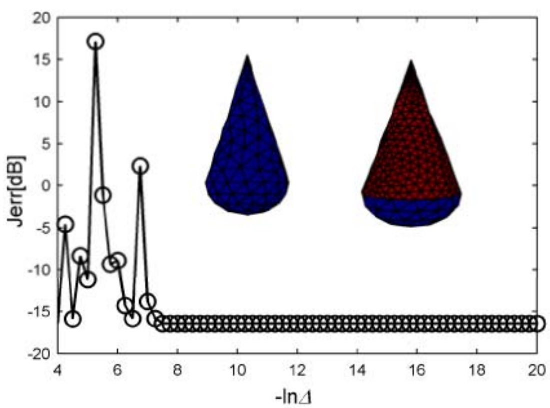

Fig. 6. Comparison of the surface current at the center points of all triangles on the mesh of the cone sphere, calculated with EFIE-DG and EFIE-RWG.

in (14), that is, perform the surface integration with respect to the field coordinates at first. It is noted in numerical experiments that the accuracy of the coefficient matrix has more effect on the solutions to EFIE-DG than to EFIE-RWG.

Example B (A PEC Cone–Sphere): The radius of the PEC hemisphere is 0.25 m, and the height of the cone is 1 m. The cone–sphere is originally meshed with a conformal triangular mesh structure with 250 triangles and 375 RWG bases and the scattering problem is solved with EFIE-RWG. Then, it is solved once again using EFIE-DG on a nonconformal triangular mesh, in which only the mesh structure on the cone surface is refined: dividing one triangle into four subtriangles by connecting the three middle points of the three edges. The cone surface has 672 triangles and the hemisphere has 82 triangles. Totally 2262 DVBFs are generated. The frequency of the incident plane wave is 1 MHz.

The two calculated results of RCS with $\Delta = l_{\min}/10$ are shown in Fig. 5. They agree well with maximum discrepancy less than 0.5 dB.

To reveal the effect of Δ, we decrease Δ from $l_{\min}/2$ to about $l_{\min}/10^7$, or equivalently to increase $(-\ln\Delta)$ approximately from 4 to 20. The surface currents at the center point of all triangles are sampled, and the relative error is shown in Fig. 6. It can be seen that the surface current obtained by using EFIE-DG approaches more close to that obtained using EFIE-RWG with larger $(-\ln\Delta)$.

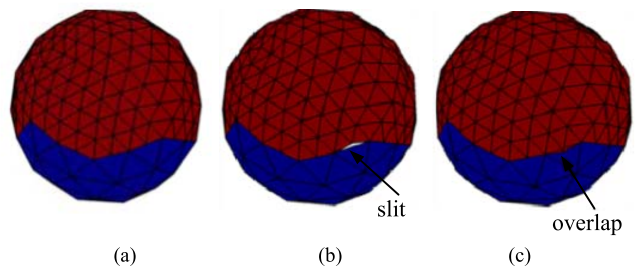

Fig. 7. PEC sphere with nonconformal meshes. (a) Normal nonconformal mesh. (b) Abnormal nonconformal mesh with a spurious slit. (c) Abnormal nonconformal mesh with a spurious overlap.

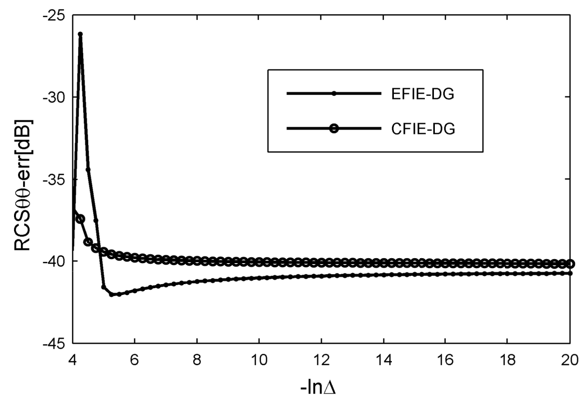

Fig. 8. Relative errors of the RCSs versus theoretical result. The SIE-DGs are solved on the normal nonconformal mesh shown in Fig. 7(a).

Example C (PEC Sphere With Nonconformal Meshes): In this example, the PEC sphere is created by combining two hemispherical surfaces with different meshes (340 triangles in the upper part and 59 triangles in the lower part), as shown in Fig. 7(a)–(c). In Fig. 7(a), the two surfaces are connected normally with their boundary contours exactly coincide, while in Fig. 7(b) and (c), the two surfaces are not perfectly connected, and there may exist some misplacements at the interfacing contour, namely, a spurious narrow slit in Fig. 7(b), and a small overlap in Fig. 7(c). Note that these displacements may be caused by importing mesh data of different parts from files generated by CAD tools. Usually these abnormal meshes have to be readjusted to get a qualified mesh structure that should make a sealed PEC sphere surface. In this example, the slit and overlap are deliberately created by shifting one node at the connecting boundary 0.04 m away from the edge it located originally. We use this example to show that the readjustment may be not necessary using SIE-DGs.

The RCS of the PEC sphere is obtained by solving the three SIE-DGs where HRWG basis functions are used, and the results associated with EFIE-DG and CFIE-DG are compared with the theoretical one obtained using Mie series expansion method, as shown in Fig. 8. It can be seen that with sufficiently small Δ, the SIE-DGs can provide satisfactorily accurate solutions.

When there is a spurious slit or an overlap in the nonconformal mesh, the SIE-DGs can be applied directly without any modifications. The frequency of the incident wave is 1 MHz.

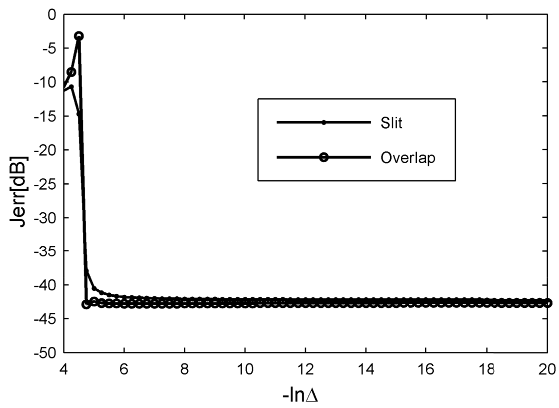

Fig. 9. Relative errors of the surface currents.

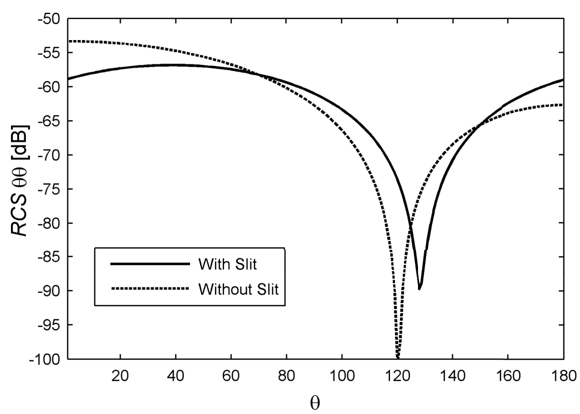

Fig. 10. RCS of a PEC sphere without slit at 1 MHz.

The surface currents obtained using the two abnormal mesh structures are sampled at the center of all triangles. They are compared with that of the normal mesh structure, as shown in Fig. 9. It can be seen that for sufficiently small Δ, the resultant surface currents agree well, which means that the effect of the misplacement tends to be very small if the DG method is employed.

For comparison, we have calculated the RCS of the PEC sphere with a real slit whose geometrical parameters are the same as the spurious one. The results are shown in Fig. 10. They are obtained with EFIE-RWG, as MFIE-RWG and CFIE-RWG are not applicable for this open structure. Fig. 10 shows that the small real slit indeed has significant effect on the scattering property of the PEC sphere.

Example D (Helicopter Model With Conformal Meshes): A PEC helicopter model, as shown in Fig. 11, is analyzed using the proposed EFIE-DG method. It is meshed with a conformal triangular mesh consisting of 4696 triangles. The ratio of the maximum edge length versus the minimum edge length is 139.5, much larger than that in *Example A*. The frequency of the incident plane wave is 100 MHz.

The relative error between the surface current coefficients obtained using the two methods is shown in Fig. 11, where Δ varies from about $l_{\min}$ to $l_{\min}/10^7$, or correspondingly, $(-\ln\Delta)$ varies from 4 to 20.

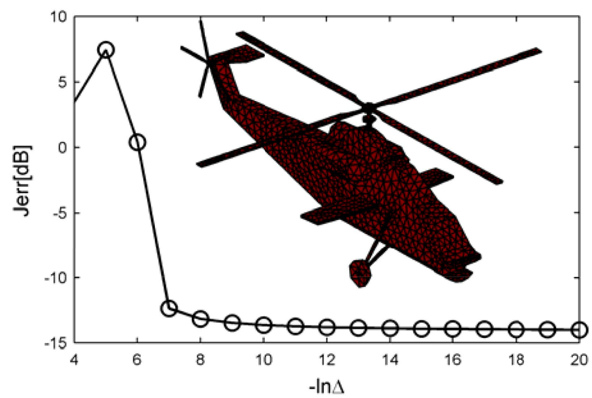

Fig. 11. Relative error of the surface current coefficients.

The relative error is about 3 dB if the double line integration is discarded as suggested in [23], which is quite larger than the proposed method here. It is possible to get higher accuracy if RWGs are used for most meshes of the surface, and DVBFs are used for the connecting interfaces. The accuracy also tends to become better for more uniform mesh structures, which is true at least in all numerical experiments we have performed.

V. Conclusion

An intuitive formulation of DG is proposed for EFIE, MFIE, and CFIE, which is obtained by simply discarding a small integration interval around the singular point in evaluating the coupling coefficients between two coincided line sources. It is verified that SIE-DGs are feasible for nonconformal meshes with possible misplacements at the connections. Numerical examples demonstrate that SIE-DGs can provide numerical results almost as accurate as SIE-RWGs. However, the condition numbers associated with SIE-DGs are usually larger than those associated with SIE-RWGs. Besides this, it seems that the low-frequency breakdown problem affects EFIE-DG more significantly than EFIE-RWG. These issues need further investigating.

References

[1] S. M. Rao, D. R. Wilton, and A. W. Glisson, "Electromagnetic scattering by surfaces of arbitrary shape," *IEEE Trans. Antennas Propag.*, vol. 30, no. 3, pp. 409–418, May 1982.

[2] H. H. Happ, "Diakoptics—The solution of system problems bytearing," *Proc. IEEE*, vol. 62, no. 7, pp. 930–940, Jul. 1974.

[3] S.-C. Lee, M. N. Vouvakis, and J.-F. Lee, "A non-overlapping domain decomposition method with non-matching grids for modeling large finite antenna arrays," *J. Comput. Phys.*, vol. 203, no. 1, pp. 1–21, Feb. 2005.

[4] L. Matekovits, V. A. Laza, and G. Vecchi, "Analysis of large complex structures with the synthetic-functions approach," *IEEE Trans. Antennas Propag.*, vol. 55, no. 9, pp. 2509–2521, Sep. 2007.

[5] S. Xiang, G. B. Xiao, X. Z. Tian, and J. Mao, "Analysis of large-scale phased antenna array with generalized transition matrix," *IEEE Trans. Antennas Propag.*, vol. 61, no. 11, pp. 5453–5464, Nov. 2013.

[6] G. A. Baker, "Finite element methods for elliptic equations using nonconforming elements," *Math. Comp.*, vol. 31, no. 137, pp. 45–59, 1977.

[7] D. N. Arnold, "An interior penalty finite element method with discontinuous elements," *SIAM J. Numer. Anal.*, vol. 19, no. 4, pp. 742–760, 1982.

[8] M. F. Wheeler, "An elliptic collocation-finite element method with interior penalties," *SIAM J. Numer. Anal.*, vol. 15, no. 1, pp. 152–161, 1978.
[9] J. S. Hesthaven and T. Warburton, "High-order accurate methods for time-domain electromagnetics," *Comput. Model. Eng. Sci.*, vol. 5, no. 5, pp. 395–407, May 2004.
[10] M. F. Wheeler, "A priori L_2 error estimates for Galerkin approximations to parabolic partial differential equations," *SIAM J. Numer. Anal.*, vol. 10, no. 4, pp. 723–759, Sep. 1973.
[11] D. N. Arnold, F. Brezzi, B. Cockburn, and L. D. Marini, "Unified analysis of discontinuous Galerkin methods for elliptic problems," *SIAM J. Numer. Anal.*, vol. 39, no. 5, pp. 1749–1779, 2002.
[12] B. Cockburn, J. Gopalakrishnan, and R. Lazarov, "Unified hybridization of discontinuous Galerkin, mixed, and continuous Galerkin methods for second order elliptic problems," *SIAM J. Numer. Anal.*, vol. 47, no. 2, pp. 1319–1365, 2009.
[13] B. Cockburn, G. E. Karniadakis, and C. W. Shu, *Discontinuous Galerkin Methods: Theory, Computation and Applications*. Tokyo, Japan: Springer-Verlag, 2000.
[14] P. Houston, I. Perugia, and D. Schötzau, "Mixed discontinuous Galerkin approximation of the Maxwell operator," *SIAM J. Numer. Anal.*, vol. 42, no. 1, pp. 434–459, 2004.
[15] E. Burman, "A unified analysis for conformal and non-conformal stabilized finite element methods using interior penalty," *SIAM J. Numer. Anal.*, vol. 43, no. 5, pp. 2012–2033, 2005.
[16] P. Houston, I. Perugia, and D. Schötzau, "Energy norm *a posteriori* error estimation for mixed discontinuous Galerkin approximations of the Maxwell operator," *Comput. Methods Appl. Mech. Eng.*, vol. 194, nos. 2–5, pp. 499–510, Feb. 2005.
[17] P. Houston, I. Perugia, and D. Schötzau, "An *a posteriori* error indicator for discontinuous Galerkin discretizations of $H(curl)$-elliptic partial differential equations," *SIAM J. Numer. Anal.*, vol. 27, no. 1, pp. 122–150, 2007.
[18] D. L. Dault, N. V. Nair, J. Li, and B. Shanker, "The generalized method of moments for electromagnetic boundary integral equations," *IEEE Trans. Antennas Propag.*, vol. 62, no. 6, pp. 3174–3188, Jun. 2014.
[19] A. Buffa, P. Houston, and I. Perugia, "Discontinuous Galerkin computation of the Maxwell eigenvalues on simplicial meshes," *J. Comput. Appl. Math.*, vol. 204, no. 2, pp. 317–333, Jul. 2007.
[20] N. V. Nair and B. Shanker, "Generalized method of moments: A novel discretization technique for integral equations," *IEEE Trans. Antennas Propag.*, vol. 59, no. 6, pp. 2280–2293, Jun. 2011.
[21] A. Bendali, F. Collino, M. Fares, and B. Steif, "Extension to non-conforming meshes of the combined current and charge integral equation," *IEEE Trans. Antennas Propag.*, vol. 60, no. 10, pp. 4732–4744, Oct. 2012.
[22] Z. Peng, K.-H. Lee, and J.-F. Lee, "A discontinuous Galerkin surface integral equation method for electromagnetic wave scattering from nonpenetrable targets," *IEEE Trans. Antennas Propag.*, vol. 61, no. 7, pp. 3617–3628, Jul. 2013.
[23] M. A. E. Bautista, F. Vipiana, M. A. Francavilla, J. A. T. Vasquez, and G. Vecchi, "A nonconformal domain decomposition scheme for the analysis of multiscale structures," *IEEE Trans. Antennas Propag.*, vol. 63, no. 8, pp. 3548–3560, Aug. 2015.
[24] N. Heuer and S. Meddahi, "Discontinuous Galerkin hp-BEM with quasi-uniform meshes," *Numer. Math.*, vol. 125, no. 4, pp. 679–703, Dec. 2013.
[25] F. R. Vipiana and D. R. Wilton, "Numerical evaluation via singularity cancellation schemes of near-singular integrals involving the gradient of Helmholtz-type potentials," *IEEE Trans. Antennas Propag.*, vol. 61, no. 3, pp. 1255–1265, Mar. 2013.
[26] P. Yla-Oijala and M. Taskinen, "Calculation of CFIE impedance matrix elements with RWG and nxRWG functions," *IEEE Trans. Antennas Propag.*, vol. 51, no. 8, pp. 1837–1846, Aug. 2003.
[27] D. R. Wilton, S. M. Rao, A. W. Glisson, D. H. Schaubert, O. Al-Bundak, and C. M. Butler, "Potential integrals for uniform and linear source distributions on polygonal and polyhedral domains," *IEEE Trans. Antennas Propag.*, vol. 32, no. 3, pp. 276–281, Mar. 1984.

Gaobiao Xiao (M'10) received the B.S. degree from the Huazhong University of Science and Technology, Wuhan, China, in 1988, the M.S. degree from the National University of Defense Technology, Changsha, China, in 1991, and the Ph.D. degree from Chiba University, Chiba, Japan, in 2002.

He was with Hunan University, Changsha, from 1991 to 1997. Since 2004, he has been a Faculty Member with the Department of Electronic Engineering, Shanghai Jiao Tong University, Shanghai, China. His current research interests include numerical methods in electro-magnetic fields, coupled thermo-electromagnetic analysis, microwave filter designs, fiber-optic filter designs, phased arrays, and inverse scattering problems.

Yibei Hou (S'15) received the B.S. degree from the University of Electronic Science and Technology of China, Chengdu, China, in 2014. He is currently pursuing the Ph.D. degree in electronic engineering with Shanghai Jiao Tong University, Shanghai, China.

His current research interests include computational electromagnetics and its application in scattering and radiation problems.